

# Ultrafast coherent excitation of a $^{40}\text{Ca}^+$ ion

D Heinrich, M Guggemos, M Guevara-Bertsch, M I Hussain, C Roos and R Blatt

Institut für Quantenoptik und Quanteninformation, Österreichische Akademie der Wissenschaften, Technikerstr. 21a, 6020 Innsbruck, Austria

Institut für Experimentalphysik, Universität Innsbruck, Technikerstr. 25, 6020 Innsbruck, Austria

E-mail: [daniel.heinrich@uibk.ac.at](mailto:daniel.heinrich@uibk.ac.at)

## Abstract.

Trapped ions are a well-studied and promising system for the realization of a scalable quantum computer. Faster quantum gates would greatly improve the applicability of such a system and allow for greater flexibility in the number of calculation steps. In this paper we present a pulsed laser system, delivering picosecond pulses at a repetition rate of 5 GHz and resonant to the  $4S_{1/2} \leftrightarrow 4P_{3/2}$  transition in  $^{40}\text{Ca}^+$  for coherent population transfer to implement fast phase gate operations. The optical pulse train is derived from a mode-locked, stabilized optical frequency comb and inherits its frequency stability. Using a single trapped ion, we implement three different techniques for measuring the ion-laser coupling strength and characterizing the pulse train emitted by the laser, and show how all requirements can be met for an implementation of a fast phase gate operation.

## 1. Introduction

Trapped ions are a promising system for the implementation of a scalable quantum computer [1, 2, 3, 4, 5]. Two-qubit entangling gate operations have been demonstrated [6, 7, 8, 9] and combined with single-qubit gates to build an elementary quantum processor [10, 11, 12]. The entangling gate operations in these experiments rely on spectroscopically-resolved motional sidebands of the ion crystals, a requirement that limits the duration of a gate operation to more than the period of motion of the ions in the trap (typically a few  $\mu\text{s}$  or more). Overcoming this limitation would advance the development of a scalable quantum computer as it would allow one to increase the number of gate operations (computational steps) that can be completed within the coherence time of the ion-qubits.

Two-qubit entangling gate operations in less than one trap period have been proposed by García-Ripoll, Zoller and Cirac in 2003 [13] using counter-propagating laser pulses. Several groups are working on its realization [14, 15] but so far only single-qubit gate operations [16, 17] and single-ion spin-motion entanglement [18] have been reported on time scales shorter than the ion oscillation period. Recently, creation of two-qubit entanglement by a train of ultrafast laser pulses within a few microseconds has been demonstrated in the ground-states of a pair of  $\text{Yb}^+$  ions [19].

Our goal, beyond the scope of this work, is to implement an ultrafast two-qubit phase gate operation [13, 25] using resonant, counter-propagating laser pulses and to complete it in less than one trap period. The scheme uses pairs of  $\pi$ -pulses for applying ion-state dependent momentum kicks to a two-ion crystal.

Figure 1 shows a level scheme of  $^{40}\text{Ca}^+$  with the levels relevant to the gate operation. We encode each qubit in two Zeeman substates of the  $4\text{S}_{1/2}$  ( $= |\downarrow\rangle$ ) and  $3\text{D}_{5/2}$  ( $= |\uparrow\rangle$ ) states of a  $^{40}\text{Ca}^+$  ion [10]. The laser pulses resonantly excite the  $4\text{S}_{1/2} \leftrightarrow 4\text{P}_{3/2}$  transition [26]. Depending on the qubits' state, each ion will either not interact with the pulses at all (qubit state  $|\uparrow\rangle$ ) or absorb one photon from the first pulse of each pair and emit a photon into the second pulse (qubit state  $|\downarrow\rangle$ ), gaining a momentum of  $2\hbar\vec{k}$  in the direction of the first pulse, where  $\vec{k}$  is the photons' wave vector. By subjecting the ion crystal to a sequence of momentum kicks and times of free evolution of the crystal in the trap potential, the ions are forced to follow different, state-dependent trajectories through phase-space. The area enclosed by these trajectories corresponds to the phase the state acquires during the pulse sequence [7]. When the relative phase between the state-pairs  $|00\rangle$ ,  $|11\rangle$  and  $|01\rangle$ ,  $|10\rangle$  is  $\pi/2$  and the pulse sequence returns both the center-of-mass and the breathing mode of motion [27] of the ion crystal to the initial state, the operation will be the desired geometric phase gate [13]. Both conditions can be met by carefully choosing the duration of the times of free evolution in the pulse sequence. In order to complete such a phase gate within one trap period, the rate  $f_\pi$  at which pairs of  $\pi$ -pulses are applied to the ions must be much larger than the trap frequency  $\nu$  [26]. In general, the larger  $f_\pi$ , the faster the gate operation can be completed.

In order for the laser system to be suitable to implement such a fast gate operation,

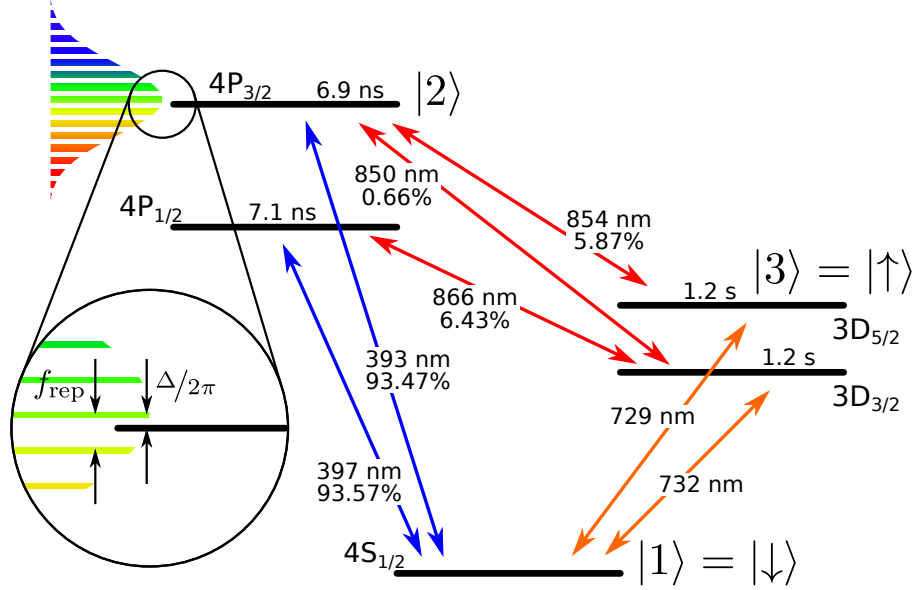


**Figure 1.** Energy level scheme of  $^{40}\text{Ca}^+$  showing the levels and transitions relevant to the experiment. Possible transitions are shown with their wavelengths and branching ratios [20, 21], excited electronic states with their lifetimes [22, 23, 24]. The bell curve-shaped bars in the upper-left corner are a representation of the pulsed laser’s spectral modes.

it should satisfy four requirements: (1) The system needs to provide pulsed laser light with a repetition rate much larger than the trap frequency of  $\sim 1$  MHz, in order to provide us with fine-grained control over the timing of pulse sequences. (2) The pulse length  $\delta t$  has to be much shorter than the  $4\text{P}_{3/2}$  state’s lifetime of 6.9 ns [22] to avoid or at least minimize spontaneous decay. (3) The center frequency has to be resonant with the  $4\text{S}_{1/2} \leftrightarrow 4\text{P}_{3/2}$  transition at 393.366 nm and (4) the laser needs to have an intensity such that for every laser pulse  $\Omega \delta t = \pi$ , where  $\Omega$  is the corresponding Rabi frequency. Alternatively to (3), non-resonant pulses can be used to apply state-dependent momentum kicks [17]. In order to realize this alternative, we want to be able to tune the laser in between the two fine structure components  $4\text{S}_{1/2} \leftrightarrow 4\text{P}_{1/2}$  and  $4\text{S}_{1/2} \leftrightarrow 4\text{P}_{3/2}$  such that Stark shifts cancel, while limiting overlap of the laser’s optical spectrum with either of the two transition frequencies.

In this paper we describe and characterize a laser system which was designed to generate the light pulses for ultrafast quantum gate operations. Our laser system satisfies requirements (1) to (3), and we will show below, that the intensity of the laser is sufficiently high for generating pulses that flip the state of the ion with 96.4(19) % probability (requirement 4). In order to do that, we present and characterize three methods to extract information on the Rabi frequency and compare them in terms of applicability and prerequisites. The methods allow us to measure the rotation angle per pulse  $\theta = \Omega \delta t$  and are more accurate than simply deducing the Rabi frequency from a measurement of the laser’s optical intensity at the point of the ion [28, 27].

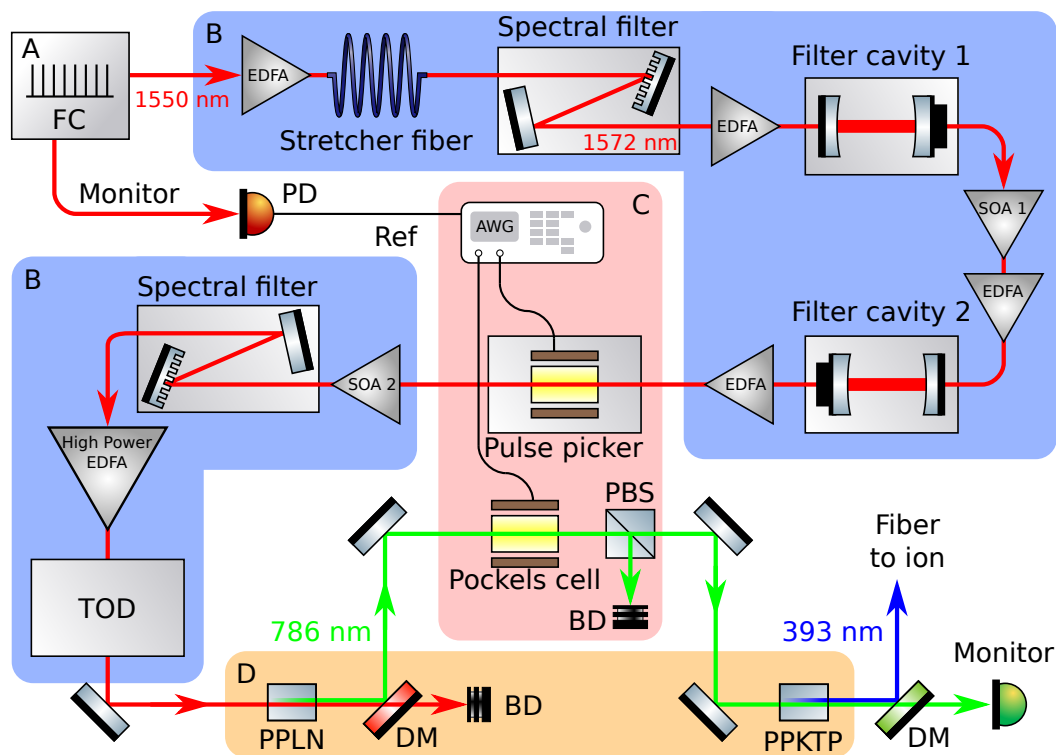


**Figure 2.** Schematic setup of our laser system. Panels marked A, B, C, D are discussed in subsections 2.1, 2.2, 2.3 and 2.4, respectively. AWG: arbitrary waveform generator, BD: Beam dump, DM: dichroic mirror, EDFA: erbium-doped fiber amplifier, FC: optical frequency comb, PBS: polarizing beam splitter, PD: photo detector, PPLN: periodically poled lithium niobate, PPKTP: periodically poled potassium titanyl phosphate, SOA: Semiconductor optical amplifier, TOD: third order dispersion compressor.

The paper is structured as follows: Section 2 describes our laser setup in detail. In section 3 we introduce two methods that we developed to gain information on  $\theta$  by carrying out measurements on a trapped  $^{40}\text{Ca}^+$  ion, and we compare them to measuring  $\theta$  by injecting single pulses between the two Ramsey zones of a Ramsey experiment [16].

## 2. Laser System

Picosecond laser systems with repetition rates on the order of GHz and a center wavelength of 393.366 nm can be constructed by frequency-quadrupling the light generated by commercial lasers operating in the L-band of optical fiber communication (1565 nm to 1625 nm). An overview of the optical setup is provided in figure 2. The system is seeded by an optical frequency comb, which is described in more detail in subsection 2.1. Filter cavities serve to multiply the laser's repetition rate. Subsequently, the desired laser wavelength range is selected by spectral filters and the laser output is amplified (subsection 2.2). Fast and slow pulse picking elements enable the selection of

arbitrary pulse sequences (subsection 2.3). Finally, the laser frequency is quadrupled by two single-pass second-harmonic generation stages (subsection 2.4). Measurements of the basic pulse characteristics are presented in subsection 2.5.

### 2.1. Seed laser

The seed laser is a fiber-based optical frequency comb (Menlo Systems FC1500-250-WG) with a repetition rate of 250 MHz. The mode locked laser creates short pulses of 70 fs pulse width with a center wavelength of 1550 nm and a spectral bandwidth of 50 nm. We lock both the carrier envelope offset and the repetition rate to a frequency reference provided by a GPS-disciplined oven-controlled crystal oscillator (Menlo Systems GPS 6-12) with a fractional frequency instability of  $\sim 2 \times 10^{-13}$ .

### 2.2. Pulse manipulation

The pulses produced by the frequency comb need to be amplified and frequency-upconverted in order to create  $\pi$ -pulses on the ions. Furthermore, the spectral bandwidth should be limited to about 1 THz ( $\hat{=} 0.5$  nm at 393 nm) to avoid residual off-resonant excitation of the  $4\text{S}_{1/2} \leftrightarrow 4\text{P}_{1/2}$  transition, and the center wavelength should be resonant to the  $4\text{S}_{1/2} \leftrightarrow 4\text{P}_{3/2}$  transition. In order to have a higher resolution of the pulse timings, we additionally multiply the repetition rate by a factor of 20.

Erbium doped fiber (pre-)amplifiers (EDFAs) and semiconductor optical amplifiers (SOAs) are used to compensate insertion loss at various stages in the set-up (panels B in figure 2). After the first preamplifier, the pulse train travels through a stretcher fiber which adds dispersion and stretches the pulses from 70 fs to  $\sim 50$  ps for chirped pulse amplification [29]. The pulse train then travels through a spectral filter which selects the new center wavelength of  $4 \cdot 393$  nm = 1572 nm and reduces the spectral bandwidth to 8 nm. Two filter cavities with a free spectral range of 5 GHz each then increase the repetition rate from 250 MHz to 5 GHz by transmitting only the light's spectral modes that are 5 GHz apart and suppressing all others. The second cavity's purpose is to increase the extinction ratio and therefore equalize optical intensity of the output pulses. The subsequent fast pulse picker (bandwidth of 7 GHz) will be described in more detail in the next subsection. Furthermore, we use a second spectral filter to compensate amplifier-induced frequency shifts [30] of up to 4 nm and further limit the bandwidth to 6.4 nm. Next, a high power EDFA amplifies the pulse train from 15 mW to a maximum average power of 2.8 W. A free-space third order dispersion compressor reduces the pulse width to 680 fs (time bandwidth product 0.53) which is close to the transform limited pulse width of 560 fs for a Gaussian-shaped pulse of the given bandwidth.

### 2.3. Pulse picking

In order to select the pulse sequences described in section 1 out of the 5 GHz pulse train, we need an optical element that is able to select pulses at this rate and to withstand up

to 2.8 W of laser power after the high power EDFA. To satisfy both requirements, we chose a twofold approach using a fast switching element before the high power EDFA (where the average laser power can be limited to 10 mW) and a slow element after the amplifier to create the desired pulse sequences (see panel C in figure 2).

The fast element is a pulse picker (custom-made ModBox by Photline) which contains a Mach-Zehnder interferometer with an electro-optic modulator of 7 GHz bandwidth. Since its maximum optical input power is on the order of a few mW, we install it before the high power EDFA where the light intensity is sufficiently low. Considering the amplifier's need to be seeded continuously with a maximally allowed dark time on the order of 20 ns, we need an additional switching element after the amplifier with a high damage threshold and a switching time of less than 20 ns. For this we use a Pockels cell (Leysop BBO-3-25-AR790) with a driver (custom-made by Bergmann Meßgeräte Entwicklung) that enables switching of the cell with a rise/fall time of 7 ns at a maximum repetition rate of 10 MHz and a measured optical extinction ratio of 30 dB. Both the pulse picker and the Pockels cell are controlled by an arbitrary waveform generator (Tektronix AWG 70002A) with a sample rate of 25 GS/s which is synchronized with the seed laser by a 250 MHz RF signal derived directly from the laser's pulse train.

Figure 3 shows three oscilloscope traces recording an arbitrary pulse pattern (including a dark time) which was detected by a photodiode. To generate the three traces, either only the pulse picker, only the Pockels cell or both were used. It shows that the pulse picker can switch individual pulses in arbitrary sequences.

#### 2.4. Frequency up conversion

The fundamental 1572 nm light is converted to 393 nm by frequency doubling the light twice in two separate nonlinear crystals (panel D in figure 2). The first one is an MgO-doped PPLN (periodically-poled lithium niobate) crystal (Covesion MSHG1550-0.5-5), the second crystal is a PPKTP (periodically-poled potassium titanyl phosphate) crystal (custom-made by Raicol Crystals Ltd.). Since the doubling efficiency of the crystals scales with the square of the peak power, the measured extinction ratio of the Pockels cell/PPKTP crystal system is 56 dB, i.e. almost the square of the Pockels cell extinction ratio. At the current maximum average 1572 nm light power of about 2.8 W and at a repetition rate of 5 GHz (1.25 GHz, and therefore four times higher peak power) we can produce 0.77 W (1.18 W) of 786 nm light, which corresponds to a conversion efficiency of 28 % (42 %), and 25 mW (110 mW) of 393 nm light, which corresponds to a conversion efficiency of the second frequency doubling step of 3.2 % (9.3 %). The maximum total conversion efficiency (from 1572 nm to 393 nm) is 0.9 % (3.9 %). Measurements of the 393 nm light power and conversion efficiencies for four different repetition rates are presented in figure 4. The inset in panel (a) of that figure is a log-log graph of the same data. The graph, together with the line  $y \propto x^4$  visualizes the expected fourth-power dependency of the 393 nm light power on the 1572 nm light power.

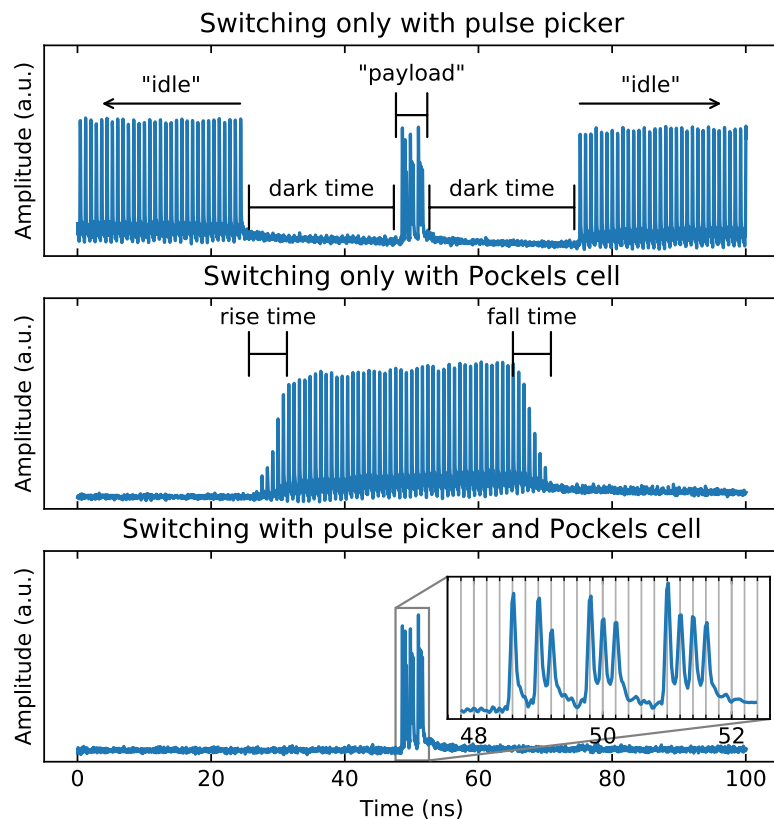


**Figure 3.** Pulse patterns generated by using either only the pulse picker (top), only the Pockels cell (middle) or both (bottom), measured by detecting the residual 786 nm light after the PPKTP crystal. The pulses labeled “idle” on both sides of the top panel are required to seed the high-power EDFA. The length of the dark time on either side of the “payload” is determined by two factors: The rise and fall times of the Pockels cell of 7 ns and the minimum allowed time of 35 ns between switching the cell on and off – i.e. between the start of the rise time and the start of the fall time. The inset in the bottom panel shows the zoomed-in payload signal. Every grid line corresponds to the location of a pulse in the original 5 GHz pulse train. For the reason for the different pulse heights see section 2.5 and especially figure 6.

After each up-conversion of the laser pulses, the remaining fundamental light is split off by a dichroic mirror and in case of the 2nd SHG stage further suppressed by a shortpass filter (Thorlabs FESH0700). Next, the light is coupled into a polarization-maintaining single-mode fiber and sent to the ion trap. After the 5 m long fiber, we measure a pulse width of 3 ps. Finally, a collimator equipped with a 250 mm lens focuses the laser beam to a waist measured to be  $w_0 = 11.8(3) \mu\text{m}$  and directs the beam such that the ion is located in the beam waist.

Unless stated otherwise, all following measurements and experiments presented in this paper were conducted at a high power EDFA output power of  $\approx 600 \text{ mW}$ . During

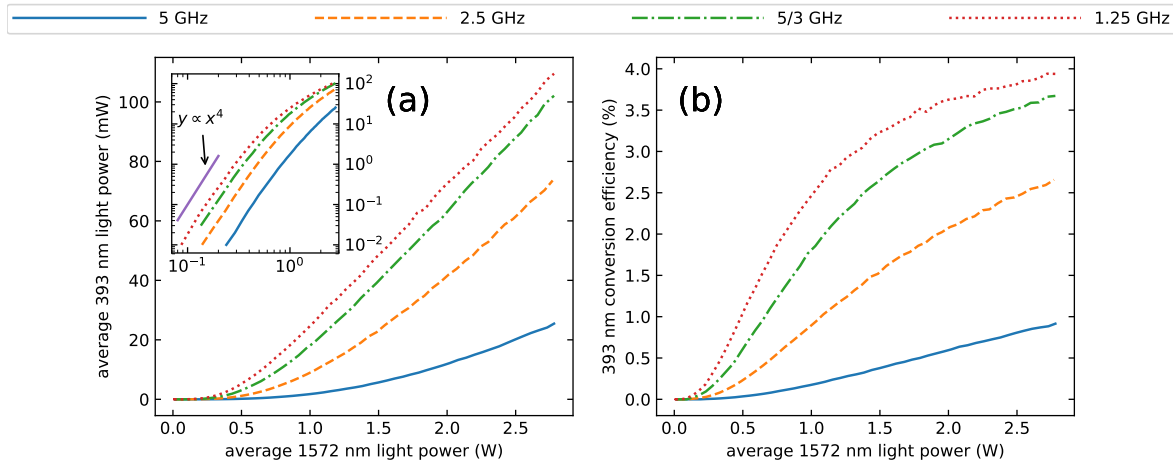


**Figure 4.** Measurement of 393 nm light power and conversion efficiencies of four different repetition rates as a function of fundamental 1572 nm light power.

times when the Pockels cell was off and the pulses directed into a beam dump, the high power EDFA was seeded with pulses at 1.25 GHz repetition rate.

### 2.5. Pulse switching characteristics

Our pulse picking scheme described in subsection 2.3 necessitates blocking the pulses with the fast pulse picker during the rise and fall time of the Pockels cell for typically 12 ns. This results in an equally long dark time of the amplifiers after the pulse picker. We examined the characteristics of the pulses during the first nanoseconds after such dark time by measuring pulse areas and relative phase of the pulses.

We characterize the phase shifts of the pulses by interfering them in a Michelson interferometer (see figure 5(a)). At the beam splitter the input pulse train is split into two copies, one of which is temporally delayed by one pulse period  $\tau_{\text{pulse}}$  with respect to the other before being recombined. In this way, every pulse  $i$  interferes with its successive pulse  $i + 1$  and the total phase difference  $\Delta\Phi_i$  of the two pulses at the output of the interferometer is a function of the phase difference  $\Delta\phi_i$  of pulses  $i$  and  $i + 1$ , and the path length difference  $\Delta x = 2x_2 - 2x_1 \approx c \cdot \tau_{\text{pulse}}$ :

$$\Delta\Phi_i = \Delta\phi_i + k \cdot \Delta x,$$

with  $x_1$  ( $x_2$ ) the length of interferometer arm 1 (2),  $c$  the speed of light and  $k$  the length of the wave vector. The interference pulses are detected on a fast photodiode and their pulse areas, which are functions of  $\Delta\Phi_i$ , extracted by integrating the photodiode's signal over the pulse length.

We can tune  $\Delta x$  by manually moving one of the retro-reflecting mirrors which is fixed on a manual translation stage, but we can not deterministically change  $\Delta x$  on a sub-wavelength scale which would have allowed to keep track of the changes in  $\Delta\Phi_i$  due to changes in  $\Delta x$ . Nevertheless, we found its fluctuations to be much smaller than the light's wavelength and consider  $\Delta x$  to be constant on time scales of our measurements



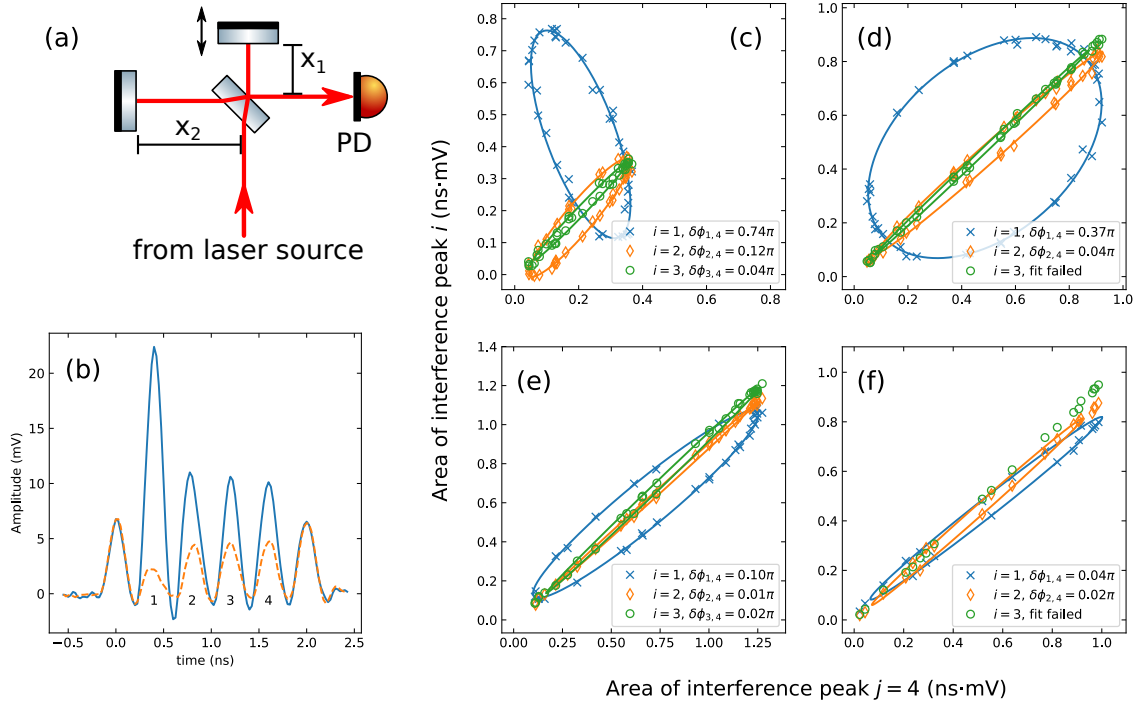


**Figure 5.** (a) Michelson interferometer for a measurement of pulse-to-pulse phase shifts. (b) Example signals at  $f_{\text{rep}} = 2.5$  GHz. The labeled peaks between 0.4 ns and 1.6 ns (four of each plot line) are interference pulses of the first four input-pulses each with its successor. (c-f): Areas of the first (blue crosses), second (yellow diamonds) and third (green circles) interference peak plotted against the area of the fourth interference peak. The solid curves are a fit of the ellipse  $\left( x(\Delta\phi) = c * \sin(\Delta\phi) + x_0, y(\Delta\phi) = c * \sin(\Delta\phi + \delta\phi_{i,j}) + y_0 \right)$  to the data, which allows us to extract  $\delta\phi_{i,j}$  up to a sign, since for  $\delta\phi_{i,j} = \Phi$  and  $\delta\phi_{i,j} = -\Phi$  the ellipses are congruent. The repetition rate is 5 GHz (c), 2.5 GHz (d), 5/3 GHz (e) and 1.25 GHz (f), respectively. For higher repetition rates, the phase difference between the first and second pulses is larger than the phase difference between later pulses. At lower repetition rates, the phase difference between any two consecutive pulses is equal within 1% of  $2\pi$ .

of about 100 ms. For each measurement we therefore randomly choose  $\Delta x$  and repeat the measurement for different  $\Delta x$ . Accordingly, the interference pulse areas of each measurement are both random but also correlated in size since  $\Delta x$  is random but equal for all pulses in a given measurement, and if the pulse areas of two interference pulses  $i$  and  $j$  are different, there is also a change  $\delta\phi_{i,j} = \Delta\phi_i - \Delta\phi_j$  in their phase differences.

In order to determine  $\delta\phi_{i,j}$  we repeatedly send a five-pulse pulse train into the interferometer at a rate of 1 kHz and average over 100 consecutive trains. We measure the interference pulse areas for different and random  $\Delta x$  by moving the translation stage back and forth on the order of  $5 \mu\text{m}$  between two 100 pulse trains-long measurements. Figure 5(b) shows two example interference signals, taken at 2.5 GHz. For every

measurement at different  $\Delta x$  we plot the pulse areas of two interference pulses against each other and present the data in panels (c) through (f) in figure 5. Every abscissa is the area of interference pulse 4; the ordinates are the areas of interference pulses 1 through 3, respectively.

The data points fall on a straight line at a  $45^\circ$  angle, if  $\delta\phi_{i,j}$  between the two interference pulses is zero or an integer multiple of  $2\pi$ , and at a  $-45^\circ$  angle if  $\delta\phi_{i,j} = (2n + 1)\pi, n \in \mathbb{Z}$ . In general, for any other value of  $\delta\phi_{i,j}$  the data points are located on an ellipse. This allows us to extract  $\delta\phi_{i,j}$  by fitting an ellipse to the data.

We see a dependence of  $\delta\phi_{i,j}$  on the length of the pulse period  $\tau_{\text{pulse}} = 1/f_{\text{rep}}$  if there was a long (here: 12 ns) dark time before the first pulse: For the maximum repetition rate of  $f_{\text{rep}} = 5$  GHz we find that between the first (second) and fourth interference peak (pulses 1&2 (2&3) and 4&5, respectively)  $\delta\phi_{1,4} = 0.74\pi$  ( $\delta\phi_{2,4} = 0.12\pi$ ). For later interference peaks ( $i \geq 3$ )  $\delta\phi_{i,4}$  is vanishingly small. As a trend we observe that for larger  $\tau_{\text{pulse}}$ ,  $\delta\phi_{i,j}$  becomes smaller and is vanishing for  $\tau_{\text{pulse}} \geq 800$  ps =  $1/1.25$  GHz.

In addition to the phase shift, we observe repetition rate-dependent deviations of the pulse intensity of the first pulses after the dark time. Figure 6 shows the pulse areas of the pulses during the first 2 ns after the dark time. In the case of 5 GHz repetition rate we observe that all pulses from the second onward are weaker by a factor of about 3 with respect to the first pulse. At 2.5 GHz repetition rate, the intensity of the second pulse decreases by about 10% with respect to the first. At the other repetition rates we do not observe this effect. For all repetition rates we observe an increase in pulse intensity of about 10% for the shown time of 2 ns of pulses after the possible initial decrease.

Both the phase shift and the change in pulse area will be problematic for experiments using coherent manipulations of the qubit. Since for our planned two-ion phase gate every pulse needs to act as a  $\pi$ -pulse, the pulse area needs to be constant, but due to the way we plan to create the counter-propagating pulse pairs, the phase shift does not: We intent to generate the two pulses of every required  $\pi$ -pulse pair by splitting a larger-area pulse. Therefore, every pulse pair will consist of identical copies and the two pulses will add up to a  $2\pi$ -rotation of the Bloch vector around the same axis regardless of phase difference with respect to other pulse pairs. For this reason only the intensity changes should pose an issue for our phase gate, the phase shifts should not.

We believe that both effects are caused by a semiconductor optical amplifier (SOA2 in figure 2) which serves as a preamplifier to the high power EDFA and are due to the finite carrier lifetime of the SOA of 500 ps. This causes the dynamical behavior of the SOA to depend on the input signal of the past  $\sim 500$  ps [31] and is known as the ‘‘pattern effect’’ [32]. We therefore plan to replace the SOA with another fiber-based preamplifier.

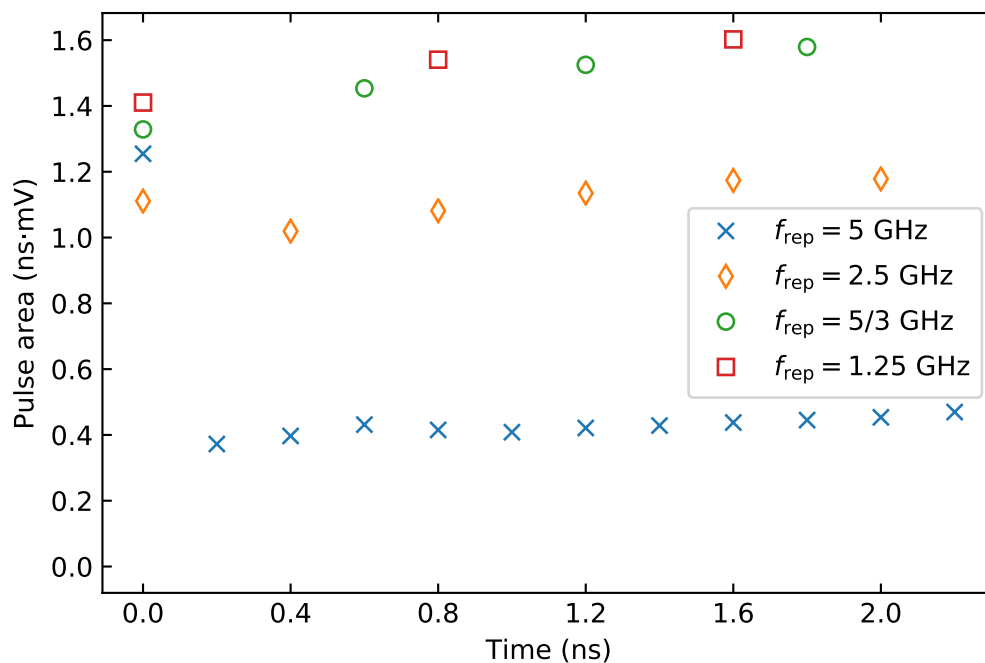


**Figure 6.** Pulse areas of pulses during the first 2 ns after a 12 ns dark time at repetition rates from 1.25 GHz to 5 GHz. Time axis relative to first pulse. Data points are the average of 1000 measurements, error bars are smaller than data point symbols. Average high power EDFA output power for this measurement was  $\approx 1.6$  W.

### 3. Methods to measure the Rabi frequency of a pulsed laser-ion system

We have employed three different techniques to measure the rotation angle per pulse  $\theta = \Omega \delta t$ . The model for the ion-laser interaction used for simulating our experiments is presented in subsection 3.1. Subsection 3.2 presents measurements using the three techniques. The first approach uses many pulses –  $\mathcal{O}(10^3)$  – to pump the ion into the metastable  $3\text{D}_{5/2}$  state. Measuring the population in that state and fitting the model to the data allows  $\theta$  to be extracted. Next, we use the same principle but in the regime of single pulses, allowing pulse dynamics and characteristics to be extracted. Finally, the third method is based on preparing the ion in a coherent superposition of the two qubit states. We then use single laser pulses to reduce and restore coherence between the qubit states by transferring population of one of the two states back and forth to a third state.

#### 3.1. Pulse model for simulation and fits

We calculate the interaction of a  $^{40}\text{Ca}^+$  ion with a pulsed laser field resonant to the ion’s  $4\text{S}_{1/2} \leftrightarrow 4\text{P}_{3/2}$  transition (see figure 1). We consider spontaneous decay of the  $4\text{P}_{3/2}$  state into the  $4\text{S}_{1/2}$  state with decay rate  $\Gamma_{\text{PS}}$  and into the  $3\text{D}_{5/2}$  state with decay rate  $\Gamma_{\text{PD}}$ . For the experiments that we describe, the  $3\text{D}_{3/2}$  state does not need to be considered as any population in this state is pumped back to  $4\text{S}_{1/2}$  via  $4\text{P}_{1/2}$  on a timescale of 10 ns

with an 866 nm laser. Therefore, any decay to  $3\text{D}_{3/2}$  effectively becomes a decay to  $4\text{S}_{1/2}$  and the modified decay rates are

$$\Gamma_{\text{PS}} = (1 - p_{5/2}) \Gamma, \quad (1)$$

$$\Gamma_{\text{PD}} = p_{5/2} \Gamma, \quad (2)$$

where  $\Gamma = \frac{1}{\tau} = \frac{1}{6.9240(19) \text{ ns}}$  [22] and  $p_{5/2} = 0.0587(2)$  the probability of  $4\text{P}_{3/2}$  to decay to  $3\text{D}_{5/2}$  [20].

Consequently, we assume a three-level system and identify the  $4\text{S}_{1/2}$  state with  $|1\rangle$ , the  $4\text{P}_{3/2}$  state with  $|2\rangle$  and the  $3\text{D}_{5/2}$  state with  $|3\rangle$ , as indicated in figure 1. Furthermore, we assume infinitesimally short pulses and neglect any decay of  $|3\rangle$ , since the  $3\text{D}_{5/2}$  state's lifetime of 1.2 s [24] is much longer than the cycle time of our experiments of about 10 ms. The system's excited state  $|2\rangle$  decays spontaneously with rates  $\Gamma_{21} \equiv \Gamma_{\text{PS}}$  and  $\Gamma_{23} \equiv \Gamma_{\text{PD}}$  into state  $|1\rangle$  and  $|3\rangle$ , respectively.

To model the time evolution of the quantum state over one pulse period of duration  $\tau_{\text{pulse}} = 1/f_{\text{rep}}$  we start with a rotation of the Bloch vector of the  $|1\rangle - |2\rangle$  subsystem around the x-axis to account for the effect of a single pulse, followed by a rotation around the z-axis to account for the detuning during the dark time between two pulses. Next, a rotation of the Bloch vector of the  $|1\rangle - |3\rangle$  subsystem around its z-axis takes into consideration an effect of the pulses on this transition's frequency. Finally, we account for spontaneous decay of state  $|2\rangle$  during the pulse period by applying the appropriate Kraus operators to the quantum state.

Hence, we start by applying an x-rotation operator  $\mathcal{U}_{\mathcal{R}}$  to a given density operator  $\rho_0$ :

$$\rho' = \mathcal{U}_{\mathcal{R}} \rho_0 \mathcal{U}_{\mathcal{R}}^\dagger, \quad (3)$$

with

$$\mathcal{U}_{\mathcal{R}} = \exp\left(\frac{i}{2} \theta (|2\rangle \langle 1| + |1\rangle \langle 2|)\right), \quad (4)$$

where  $\theta$  is the rotation angle.

Next, we allow for a possible detuning  $\Delta$  of the laser light with respect to the  $1 \leftrightarrow 2$  transition and a shift  $\Delta'$  of the state  $|3\rangle$  by applying a z-rotation  $\mathcal{U}_{\mathcal{Z}}$  to the result. Here, the angle of rotation is proportional to  $\tau_{\text{pulse}}$ ,  $\Delta$  and  $\Delta'$ , respectively:

$$\rho'' = \mathcal{U}_{\mathcal{Z}} \rho' \mathcal{U}_{\mathcal{Z}}^\dagger, \quad (5)$$

with

$$\mathcal{U}_{\mathcal{Z}} = \exp(\mathcal{Z}), \quad (6)$$

$$\mathcal{Z} = \frac{i}{2} [\Delta (|1\rangle \langle 1| - |2\rangle \langle 2|) + \Delta' (|1\rangle \langle 1| - |3\rangle \langle 3|)] \tau_{\text{pulse}}. \quad (7)$$

Finally, we calculate the Kraus operators  $\mathcal{N}$ ,  $\mathcal{D}$  to allow for spontaneous decay of the excited state  $|2\rangle$ :

$$\mathcal{N} = |1\rangle \langle 1| + \sqrt{1 - p - q} |2\rangle \langle 2| + |3\rangle \langle 3|, \quad (8)$$

$$\mathcal{D} = \sqrt{p} |1\rangle \langle 2| + \sqrt{q} |3\rangle \langle 2|, \quad (9)$$

$$\rho''' = \mathcal{N} \rho'' \mathcal{N}^\dagger + \mathcal{D} \rho'' \mathcal{D}^\dagger, \quad (10)$$

with

$$p = 1 - \exp(-\Gamma_{21} \tau_{\text{pulse}}), \quad (11)$$

$$q = 1 - \exp(-\Gamma_{23} \tau_{\text{pulse}}). \quad (12)$$

Calculating the decay of the excited state only after applying the x- and z-rotation operators is acceptable, since the pulse length of 3 ps is very short compared to the state's lifetime of 6.9 ns, and the z-rotation and decay do not influence each other.

To find the density operator  $\rho_n$  after a train of  $n$  pulses we iteratively apply these operators  $n$  times

$$\rho_n = \mathcal{N} \mathcal{U}_z \mathcal{U}_R \rho_{n-1} \mathcal{U}_R^\dagger \mathcal{U}_z^\dagger \mathcal{N}^\dagger + \mathcal{D} \mathcal{U}_z \mathcal{U}_R \rho_{n-1} \mathcal{U}_R^\dagger \mathcal{U}_z^\dagger \mathcal{D}^\dagger \quad (13)$$

and finish the calculation by letting state  $|2\rangle$  decay completely. From the resulting density operator we can easily calculate experimentally accessible observables such as populations  $\text{Tr}(|1\rangle \langle 1| \rho_n)$ ,  $\text{Tr}(|3\rangle \langle 3| \rho_n)$  and coherences  $\text{Tr}(|1\rangle \langle 3| \rho_n)$ ,  $\text{Tr}(|3\rangle \langle 1| \rho_n)$ .

To account for our observations described in section 2.5 we allow the first pulse in a pulse train to have a different (usually higher) peak power and therefore allow for its rotation angle  $\theta^{1\text{st}}$  to be different. Additionally, we allow the first pulse to turn the Bloch vector of the subsystem around an axis in the equatorial plane rotated by  $\delta\phi_{1,4}$  from the x-axis to account for its phase offset relative to the other pulses. We therefore replace  $\mathcal{R}$  with  $\mathcal{R}^{1\text{st}}$  in equation 4:

$$\mathcal{R} \rightarrow \mathcal{R}^{1\text{st}} = \frac{i}{2} \theta^{1\text{st}} (\cos(\delta\phi_{1,4}) \sigma_x^{12} + \sin(\delta\phi_{1,4}) \sigma_y^{12}). \quad (14)$$

### 3.2. Experimental results

Experiments are conducted in the same linear Paul trap as described in [33]. Its trap axis is aligned with the quantization axis defined by a bias magnetic field. Circularly polarized 393 nm laser pulses that are sent through the holes in the trap's endcap electrodes therefore couple only pairs of Zeeman states of the ground and excited state.

*3.2.1. Pumping into a dark state with many pulses.* We send pulse trains of between 500 and 5000 pulses to the Doppler-cooled and optically pumped ion and collect fluorescence photons on the  $4\text{S}_{1/2} \leftrightarrow 4\text{P}_{1/2}$  transition in order to determine whether the ion has decayed into the dark  $3\text{D}_{5/2}$  state. We repeat the measurement 100 times to statistically determine the probability that the ion has decayed into the  $3\text{D}_{5/2}$  state. Due to the large number of pulses, the pulse switching effects described in section 2.5 and which are affecting only the first one or two pulses, can be disregarded. For the same reason the experiment does not necessitate the use of a pulse picker that is faster than the fundamental repetition rate.

We measure the  $3\text{D}_{5/2}$  state population  $P_{\text{D}}$  as a function of the laser detuning for different pulse train lengths. Figure 7 shows data sets for repetition rates ranging from 1.25 GHz to 5 GHz. Each data set consists of four data sub-sets which differ only in the number of pulses. In order to extract  $\theta$  we fit the simulation in equation (13) simultaneously to each of the four sub-sets such that we get a single value for  $\theta$ . The only other fit parameter is a detuning offset which is eliminated in the figure. For the repetition rate of 5 GHz (2.5 GHz, 5/3 GHz, 1.25 GHz) we obtain  $\theta = 0.227(12)\pi$  ( $0.323(5)\pi$ ,  $0.363(5)\pi$ ,  $0.345(5)\pi$ ).

*3.2.2. Pumping into a dark state with single pulses.* In order to implement our phase gate scheme we need to ensure that every single pulse is a  $\pi$ -pulse and it does not suffice to characterize an ensemble of hundreds of pulses. By instead sending only  $n \leq 12$  pulses at a time to the ion we can gain crucial insights into single pulse dynamics and characteristics. In order to prevent the problem of having to measure very small  $3\text{D}_{5/2}$  state populations, we amplify the signal by repeating the pulse train  $m = 20$  times as shown in the experimental sequence in figure 8. Between repetitions, a waiting time  $t_{\text{w}} = 20 \mu\text{s}$  much larger than the  $4\text{P}_{3/2}$  state's lifetime  $\tau = 6.924 \text{ ns}$  ensures that any population in that state has decayed and we accumulate population in the  $3\text{D}_{5/2}$  state [20].

Figure 9 shows the probability for being in the  $3\text{D}_{5/2}$  state, inferred from our experimental data and fit/simulation side-by-side. We vary the detuning  $\Delta$  and the number of pulses for different repetition rates. Free fit parameters are  $\theta$ , the phase offset of the first pulse  $\delta\phi_{1,4}$  and a detuning offset. Since we know from earlier measurements described in section 2.5 that the first pulse in the case of 5 GHz repetition rate has a different area than the other pulses, we allow an additional fit parameter in that case: the rotation angle of the first pulse  $\theta^{1\text{st}}$ . All fit values are within three standard deviations of those acquired previously with long pulse trains (section 3.2.1), as well as those acquired with the Michelson interferometer (section 2.5). Contrary to measuring  $\delta\phi_{i,j}$  with the interferometer, this measurement is able to also determine the sign of  $\delta\phi_{i,j}$  and therefore to distinguish between phases  $\delta\phi_{i,j} = \Phi$  and  $\delta\phi_{i,j} = -\Phi$  (the later being the same as  $\delta\phi_{i,j} = 2\pi - \Phi$ ). We therefore assume that  $\delta\phi_{1,4}$  at 5 GHz is about  $1.25\pi$  and not  $0.75\pi$  as the ellipse fit suggested. Furthermore,  $\theta^{1\text{st}}$  is found to be a factor of about  $\sqrt{3}$  larger than  $\theta$  for the 5 GHz repetition rate, which is the expected amount for a three times larger pulse area (also compare with section 2.5).

*3.2.3. Single pulse with area  $\pi$ .* In order to check if a single pulse can act as a  $\pi$ -pulse we repeat the previous experiment with only a single pulse while varying the 393 nm light power ( $n = 1$ ,  $m = 15$ ). From the experimentally determined  $3\text{D}_{5/2}$  state probability  $P_{\text{D}}$  after the 15 repetitions of a single pulse we calculate the  $4\text{P}_{3/2}$  state probability  $P_{\text{P}}$  after only one single pulse using

$$P_{\text{P}} = \frac{1}{0.0587} \left( 1 - (1 - P_{\text{D}})^{\frac{1}{m}} \right). \quad (15)$$

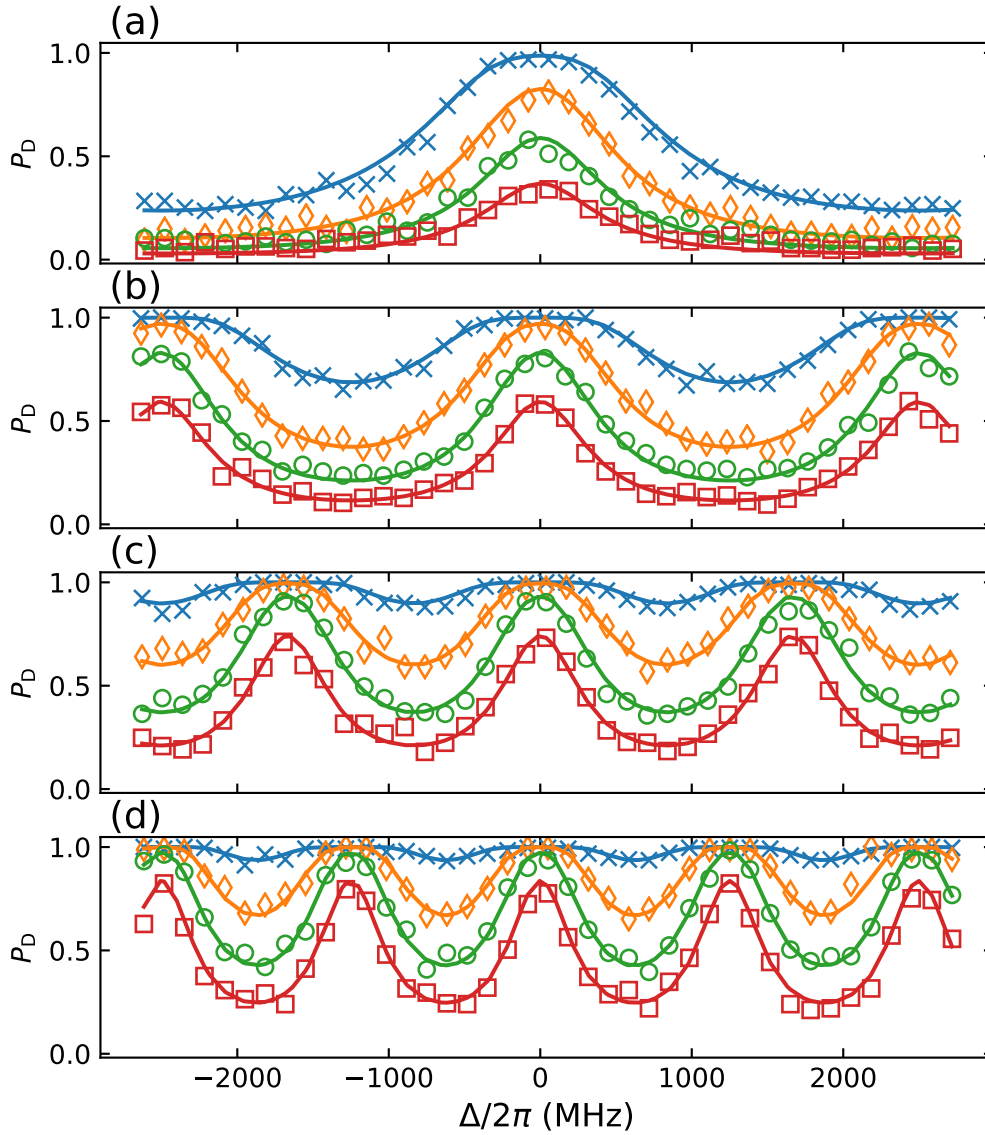


**Figure 7.** Probability  $P_D$  to find the ion in the  $3D_{5/2}$  state as a function of the detuning  $\Delta$  of the laser frequency with respect to the  $4S_{1/2} \leftrightarrow 4P_{3/2}$  transition frequency. Blue crosses using 5000 pulses, yellow diamonds 2000 pulses, green circles 1000 pulses, red squares 500 pulses. The lines in each graph are a model fit to the respective data as described in the text, allowing the determination of  $\theta$  (a) 5 GHz repetition rate, for which we find  $\theta = 0.227(12)\pi$ . (b) 2.5 GHz repetition rate,  $\theta = 0.323(5)\pi$ . (c) 5/3 GHz repetition rate,  $\theta = 0.363(5)\pi$ . (d) 1.25 GHz repetition rate,  $\theta = 0.345(5)\pi$ .

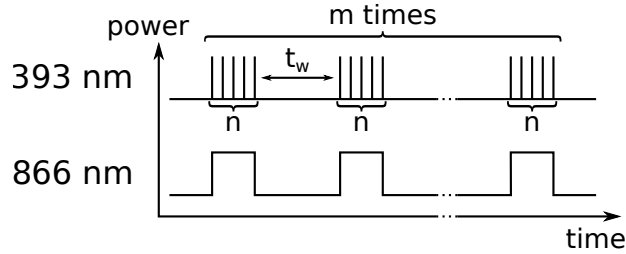


**Figure 8.** Experimental sequence of dark state pumping with single pulses. The ion is Doppler-cooled and prepared in the  $4S_{1/2}$  state. A pulse train of  $n$  pulses coherently drives the  $4S_{1/2} \leftrightarrow 4P_{3/2}$  transition. The pulse train is repeated a total of  $m = 20$  times with a waiting time  $t_w$  between each two repetitions. We choose  $t_w = 20 \mu\text{s} \gg \tau = 6.924 \text{ ns}$  with  $\tau$  the  $4P_{3/2}$  state's lifetime. Finally, we measure the  $3D_{5/2}$  state probability.

Due to measurement fluctuations, this can sometimes lead to unphysical values of  $P_P > 1$  if we measure a  $P_D$  that happens to be larger than the maximum expectation value of  $P_{D, \text{max}} = 1 - (1 - 0.0587)^{15} \approx 0.60$ .

Since the excitation probability is a function of the sine squared of the Rabi frequency  $\Omega$ , we plot  $P_P$  versus the square root of the 393 nm light power, which is proportional to  $\Omega$  (and  $\theta$ ) in figure 10. The data points should therefore follow the curve

$$P_P = P_{P, \text{max}} \cdot \sin^2(\sqrt{P_{\text{light}}}/\omega), \quad (16)$$

where  $\omega$  is a proportionality factor of dimension  $\sqrt{\text{W}}$  and  $P_{P, \text{max}}$  is the maximum probability of a single pulse exciting the ion to the  $4P_{3/2}$  state. A fit of this curve to our data yields  $P_{P, \text{max}} = 96.4(19) \%$ , showing how close we are to achieving single pulse  $\pi$ -pulses.

Please note that the maximum 393 nm light power plotted in figure 4 (e) (110 mW) and figure 10 ( $(7.6 \sqrt{\text{mW}})^2 \approx 58 \text{ mW}$ ) was measured at the same fundamental light power. The discrepancy is due to coupling losses in the fiber guiding the 393 nm light to the ion.

*3.2.4. Ramsey contrast decay and revival.* In experiments using coherent manipulations of the qubit it is important to know the effect of the manipulation on the relative phase of the two qubit states. The experiments of the previous three subsections used only one of the two qubit states and the relative phase appeared only as an unobservable global phase. Here however, the second qubit state serves as a phase reference, giving us access to the desired information.

We let single pulses interact with the ion during the waiting time of a Ramsey experiment and monitor the coherence at the end of the Ramsey sequence in the following way: We start by bringing the ion into a coherent superposition of two states by a  $\frac{\pi}{2}$ -pulse on the  $4S_{1/2} \leftrightarrow 3D_{5/2}$  transition with a 729 nm laser as illustrated in figure



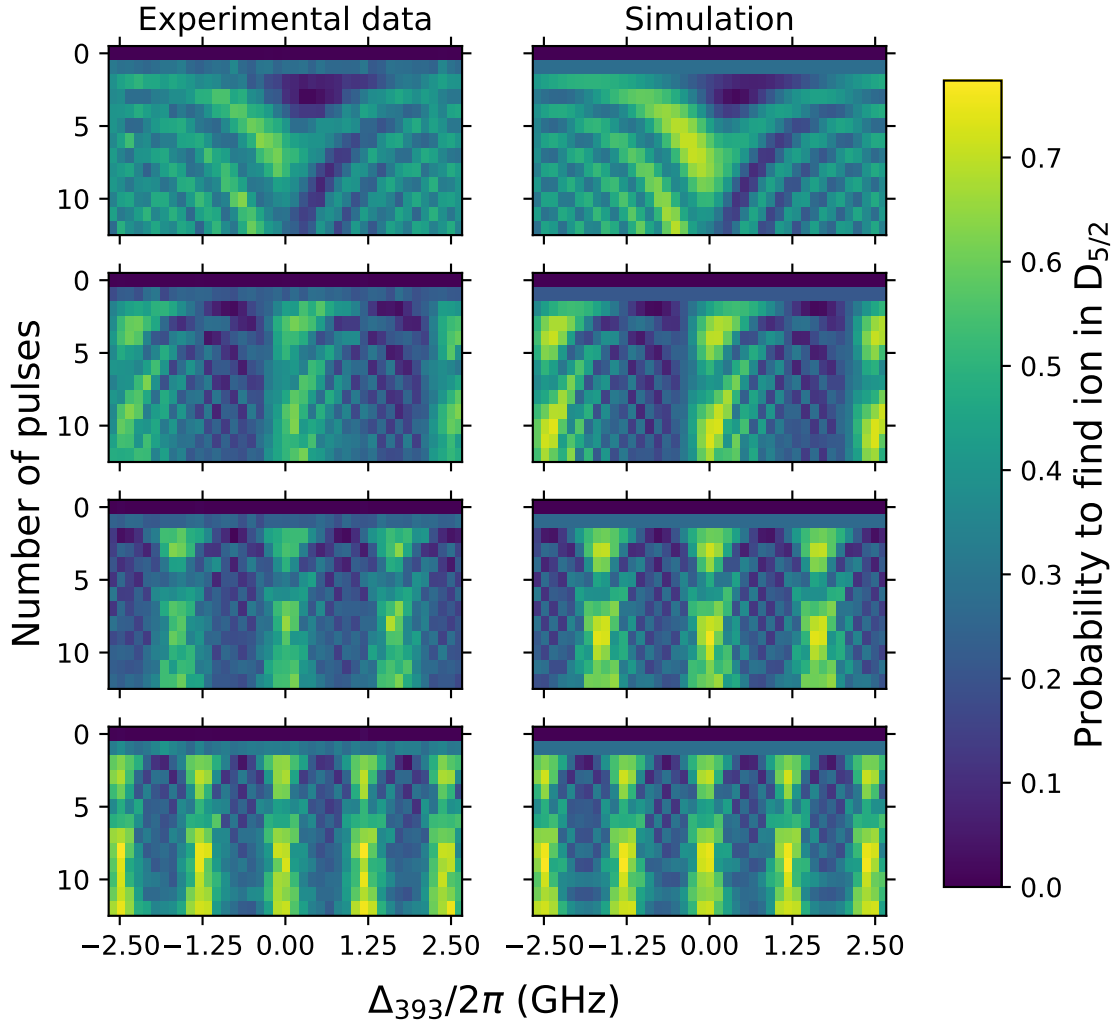


**Figure 9.** Probability to excite the ion to  $3D_{5/2}$  with different number of pulses and detuning. Left column: experimental data; right column: simulation/fit. 1st row: 5 GHz repetition rate,  $\theta^{1\text{st}} = 0.353(1)\pi$ ,  $\theta = 0.195(18)\pi$ ,  $\delta\phi_{1,4} = 1.282(1)\pi$ . 2nd row: 2.5 GHz repetition rate,  $\theta = 0.312(10)\pi$ ,  $\delta\phi_{1,4} = 0.361(2)\pi$ . 3rd row: 5/3 GHz repetition rate,  $\theta = 0.339(7)\pi$ ,  $\delta\phi_{1,4} = 0.088(3)\pi$ . 4th row: 1.25 GHz repetition rate,  $\theta = 0.358(3)\pi$ ,  $\delta\phi_{1,4} = 0.051(1)\pi$ . The asymmetry evident in the first two rows is due to the phase shift of the first pulse with respect to later pulses.

11:

$$|\psi\rangle = \frac{1}{\sqrt{2}} (|1\rangle + |3\rangle) \equiv \frac{1}{\sqrt{2}} (|4S_{1/2}\rangle + |3D_{5/2}\rangle)$$

We then use single pulses of our 393nm laser system to coherently drive the  $4S_{1/2} \leftrightarrow 4P_{3/2}$  transition. If there is any population remaining in the  $4P_{3/2}$  state after the pulses, this part of the population will undergo spontaneous decay and thus destroy the coherence. We finally analyze how much coherence of the original state remains and also extract the phase between the two states.

In mathematical terms, let  $\rho$  be the density matrix describing our system after the

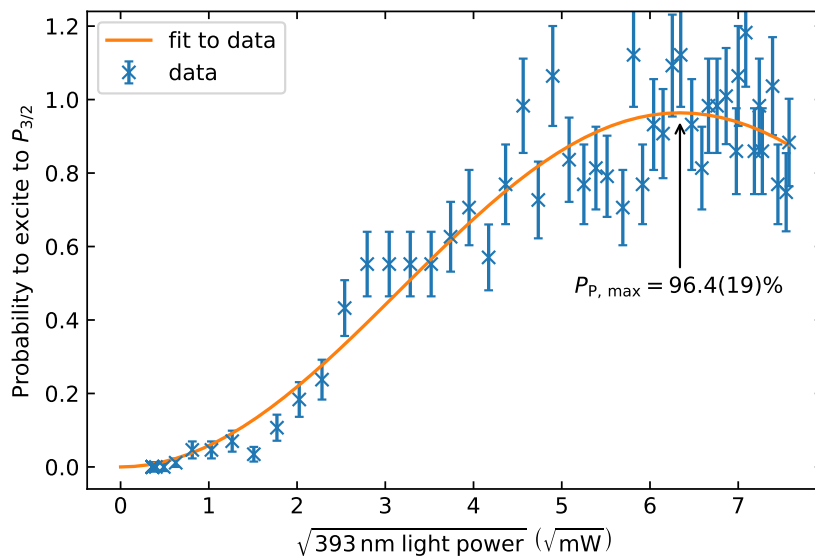


**Figure 10.** Probability to excite the ion to  $4P_{3/2}$  with a single pulse as a function of 393 nm light power.  $P_{P, \max}$  is the maximum excitation probability to the  $4P_{3/2}$  state and determined by a fit to the data. Measurement noise can cause unphysical values of  $P_P > 1$  (see text).

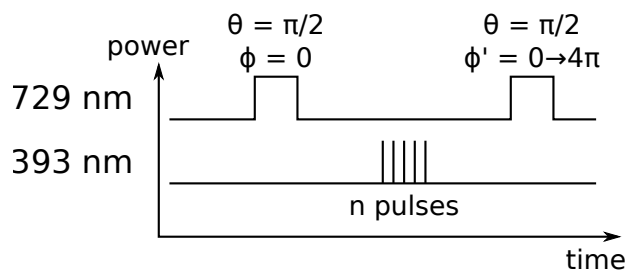


**Figure 11.** Sequence of a Ramsey contrast decay and revival experiment. The ion is Doppler-cooled and prepared in the  $4S_{1/2}$  state. The first 729 nm laser pulse creates a coherent superposition of the ion's internal  $4S_{1/2}$  and  $3D_{5/2}$  states. A controlled and variable number of 393 nm laser pulses act on the remaining  $4S_{1/2}$  state population, transferring population to the  $4P_{3/2}$  state and possibly back, potentially reducing the S-D coherence. We finally analyze how much coherence remains by varying the phase of the second 729 nm laser pulse and measuring the  $3D_{5/2}$  state probability, while keeping the Ramsey time  $t_R = 10 \mu\text{s}$  much shorter than the coherence time of the superposition ( $\mathcal{O}(1 \text{ ms})$ ).

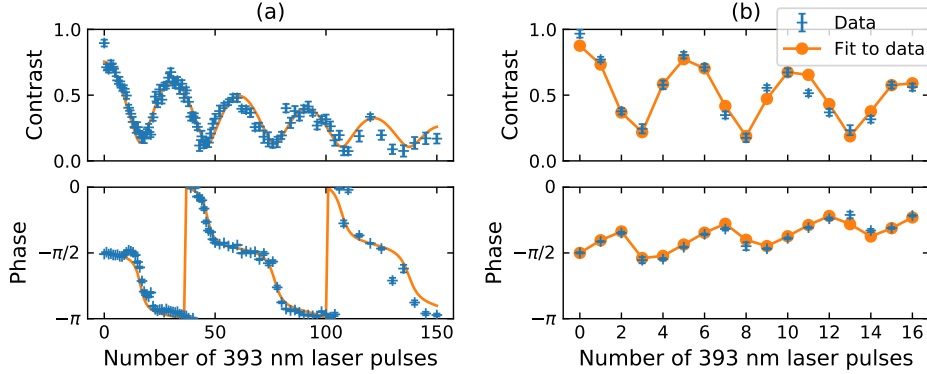


**Figure 12.** Contrast and phase of the experiment described in figure 11. Each pair of contrast/phase data points was obtained by a two-step process: For a given number of 393 nm laser pulses the experiment was repeated 100 times for each of 41 different phases from 0 to  $4\pi$ . Then the contrast and phase were extracted from a fit to that data. This was repeated for each number of laser pulses. The solid circles and the connecting curve were computed using equations (13), (17) and (18), and the parameters determined by a fit to the data. Additionally, the contrast is scaled by another fit parameter  $C$  to accommodate the reduced contrast, which we believe is caused by unwanted leaking light during the experiment. (a) Data set taken at a repetition rate of 5 GHz at low light power ( $\theta = 0.065\pi$ ,  $\Delta = 0.03159$  GHz,  $\Delta' = -0.003626$  GHz,  $C = 0.7541$ ). (b) Data set taken at 1.25 GHz repetition rate. We determine  $\theta = 0.377\pi$ ,  $\Delta = 0.1310$  GHz,  $\Delta' = -0.1866$  GHz,  $C = 0.8761$ .

393 nm pulses and  $\sigma_x^{\text{SD}}$ ,  $\sigma_y^{\text{SD}}$  the Pauli matrices acting only on the states  $|4S_{1/2}\rangle$  and  $|3D_{5/2}\rangle$  of the three level system. The expected contrast  $C$  and phase  $\Phi$  can then be written as

$$C = \sqrt{\text{Tr}^2(\sigma_x^{\text{SD}}\rho) + \text{Tr}^2(\sigma_y^{\text{SD}}\rho)}, \quad (17)$$

$$\Phi = \arg [\text{Tr}(\sigma_x^{\text{SD}}\rho) + i \text{Tr}(\sigma_y^{\text{SD}}\rho)]. \quad (18)$$

Measuring  $P_{D_{5/2}}$  as a function of the phase  $\phi'$  of the second  $\frac{\pi}{2}$ -pulse allows us to fit a sinusoidal curve to the data and extract contrast and phase from the fit. If the contrast is equal to one the ion was still in a fully coherent superposition of the  $4S_{1/2}$  and  $3D_{5/2}$  states and there was no spontaneous decay of the  $4P_{3/2}$  state. If the contrast is zero all the initial  $4S_{1/2}$  state population had been transferred to the  $4P_{3/2}$  state and the inevitable spontaneous decay had destroyed all coherence. The phase on the other hand is expected to undergo jumps of value  $\pi$  each time the ion's state population is transferred to the  $4P_{3/2}$  state and back again to the  $4S_{1/2}$  state by the pulse train. This is due to the fact that a two-level system picks up a sign after a  $2\pi$  rotation  $|0\rangle \xrightarrow{2\pi} -|0\rangle$ .

We repeat the measurement as a function of the number  $n$  of 393 nm laser pulses. Figure 12 (a) shows a data set where we plot the remaining coherence and phase against the number of pulses. For this set it took about 15 optical pulses at 5 GHz repetition rate to complete a  $\pi$ -pulse, which corresponds to  $\theta \approx 0.067\pi$ . Nevertheless, one can already see that we can drive the  $4S_{1/2} \leftrightarrow 4P_{3/2}$  transition coherently and that each

**Table 1.** Summary of fit parameters for the different experiments

Rep. rate (GHz)	Experiment	$\theta$ ( $\pi$ )	$\delta\phi_{1,4}$ ( $\pi$ )
5	interferometer		0.74 or 1.26
	many pulses	0.227(12)	
	single pulses	0.195(18)	1.282(1)
2.5	interferometer		0.37
	many pulses	0.323(5)	
	single pulses	0.312(10)	0.361(2)
5/3	interferometer		0.10
	many pulses	0.363(5)	
	single pulses	0.339(7)	0.088(3)
1.25	interferometer		0.04
	many pulses	0.345(5)	
	single pulses	0.358(3)	0.051(1)
	Ramsey exp.	0.377(5)	

time we return to the  $4S_{1/2}$  state, the data is consistent with the observation of phase jumps by  $\pi$ .

In figure 12 (b) we plot the same quantities of another data set taken at the same laser power as the measurements presented in the other subsections. We can observe the same structure as in the first data set but we need only about 2.5 optical pulses to complete one  $\pi$ -pulse on the transition. A fit of the simulation of the ion-light interaction to the experimental data allows us to extract  $\theta = 0.389(5)\pi$ .

### 3.3. Discussion

As shown above, we were able to deduce the rotation angle per pulse  $\theta$  by letting an ion interact with hundreds of consecutive pulses and afterwards measuring the probability of finding the ion in the  $3D_{5/2}$  state. Using only single pulses allowed us to measure not only  $\theta$  again, but also the phase offset of the first pulse after a dark time, i.e. a pause in the pulse train. By injecting single pulses into the waiting time between the two  $\pi/2$ -pulses of a Ramsey experiment, we were able to gain information on how the pulses influence the phase of the  $|4S_{1/2}\rangle$  state as well as measure  $\theta$ .

We now have three reliable ways to measure  $\theta$  and the phase offset of the first pulses after a dark time. The methods produce the same results within their respective error margins but each have their advantages and disadvantages as described below. Table 1 summarizes our results.

Using many pulses to pump into a dark state allows us to measure the laser-ion system's rotation angle per pulse  $\theta$  and requires neither the ability to pick single pulses nor a laser resonant to the  $4S_{1/2} \leftrightarrow 3D_{5/2}$ , 729 nm, 1 Hz linewidth, quadrupole transition. We therefore only need additional lasers that are readily available and only need to be

stabilized to a linewidth of  $\lesssim 1$  MHz, which can be achieved easily. The only parameters that need to be known to fit the data are the number of pulses  $n$  and the well-known decay rates  $\Gamma_{\text{PS}}$  and  $\Gamma_{\text{PD}}$ . From the fit we can extract  $\theta$  and also the detuning between the transition frequency and a laser mode. This allows us to tune the laser into resonance with the transition.

The method works well for any laser repetition rate  $f_{\text{rep}}$  as long as it is much larger than the  $4\text{S}_{1/2} \leftrightarrow 4\text{P}_{3/2}$  transitions linewidth. Also, the rotation angle should satisfy  $\theta \leq \pi$ , since rotation angles  $\theta' = \pi + \delta$  can not be discerned from  $\theta = \pi - \delta$ .

By using only single pulses to pump into a dark state (method 2) we can observe single pulse dynamics and gain additional information about the pulse characteristics, such as changing phase shifts and pulse powers. With these measurements we are able to reproduce results obtained both with long pulse trains and with the Michelson interferometer.

The Ramsey contrast technique (method 3) is experimentally more challenging than the previous procedures. We need to be able to create a coherent superposition of the  $4\text{S}_{1/2}$  and  $3\text{D}_{5/2}$  states which requires a few-kHz linewidth laser. It is also necessary that any AC Stark shift has been canceled, otherwise it is not possible to transfer all  $4\text{S}_{1/2}$  state population to the  $4\text{P}_{3/2}$  state as required. The advantage is that we can immediately see if we have reached our goal and if one pulse suffices to do a  $\pi$ -pulse on the ion. By fitting an empirical model to the data we can also learn how many pulses are currently needed to do a  $\pi$ -pulse, if the power is not sufficient, yet. Furthermore, the method allows one to track the phase of the population in the  $4\text{S}_{1/2}$  state because the  $3\text{D}_{5/2}$  state population serves as a phase reference.

A fourth method [34] exists that we have not pursued systematically. It is based on measuring the fluorescence rate of the ion while it is interacting with a continuous pulse train. While it is experimentally easy to conduct, it requires precise knowledge of the detector's total efficiency.

As stated before, almost all experiments presented in this work were conducted at an average output power of the high power EDFA of  $\approx 600$  mW which corresponds to  $\approx 10$  mW 393 nm light power. Nevertheless, we are able to increase the 393 nm light power to  $\gtrsim 100$  mW as seen in figure 4, which suffices to create pulses that act as  $\pi$ -pulses with 96.4(19) % probability.

## 4. Conclusion

In summary, we have designed, set up and characterized a high repetition rate laser, derived from a stabilized optical frequency comb, which is suitable for the implementation of ultrafast quantum gate operations with trapped  $^{40}\text{Ca}^+$  ions. We amplify the light at 1572 nm and shift the wavelength via cascaded SHG to 393 nm, resonant to the  $4\text{S}_{1/2} \leftrightarrow 4\text{P}_{3/2}$  transition in  $^{40}\text{Ca}^+$ . We have demonstrated that we can pick arbitrary pulse sequences out of the 5 GHz pulse train and that our laser can coherently drive the  $4\text{S}_{1/2} \leftrightarrow 4\text{P}_{3/2}$  transition in  $^{40}\text{Ca}^+$ .

We have developed and applied three different techniques to measure the rotation angle per pulse  $\theta = \Omega \delta t$  of a pulsed laser-ion system and shown that we can create approximate  $\pi$ -pulses on the  $4\text{S}_{1/2} \leftrightarrow 4\text{P}_{3/2}$  transition with only a single optical pulse: a key-requisite to implementing a resonant, ultrafast, two-qubit phase gate operation.

## References

- [1] Cirac J I and Zoller P 1995 *Phys. Rev. Lett.* **74** 4091–4094
- [2] Kielpinski D, Monroe C and Wineland D J 2002 *Nature* **417** 709–711
- [3] Wineland D J, Barrett M, Britton J, Chiaverini J, DeMarco B, Itano W M, Jelenkovic B, Langer C, Leibfried D, Meyer V, Rosenband T and Schatz T 2003 *Philos. Trans. R. Soc. A Math. Phys. Eng. Sci.* **361** 1349–1361
- [4] García-Ripoll J J, Zoller P and Cirac J I 2005 *J. Phys. B At. Mol. Opt. Phys.* **38** S567–S578
- [5] Häffner H, Roos C and Blatt R 2008 *Phys. Rep.* **469** 155–203
- [6] Schmidt-Kaler F, Häffner H, Riebe M, Gulde S, Lancaster G P T, Deuschle T, Becher C, Roos C F, Eschner J and Blatt R 2003 *Nature* **422** 408–411
- [7] Leibfried D, DeMarco B, Meyer V, Lucas D, Barrett M, Britton J, Itano W M, Jelenković B, Langer C, Rosenband T and Wineland D J 2003 *Nature* **422** 412–415
- [8] Ballance C J, Harty T P, Linke N M, Sepiol M A and Lucas D M 2016 *Phys. Rev. Lett.* **117** 060504
- [9] Gaebler J P, Tan T R, Lin Y, Wan Y, Bowler R, Keith A C, Glancy S, Coakley K, Knill E, Leibfried D and Wineland D J 2016 *Phys. Rev. Lett.* **117** 060505
- [10] Schmidt-Kaler F, Häffner H, Gulde S, Riebe M, Lancaster G P T, Deuschle T, Becher C, Hänsel W, Eschner J, Roos C F and Blatt R 2003 *Appl. Phys. B* **77** 789–796
- [11] Schindler P, Nigg D, Monz T, Barreiro J T, Martinez E, Wang S X, Quint S, Brandl M F, Nebendahl V, Roos C F, Chwalla M, Henrich M and Blatt R 2013 *New J. Phys.* **15** 123012
- [12] Debnath S, Linke N M, Figgatt C, Landsman K A, Wright K and Monroe C 2016 *Nature* **536** 63–66
- [13] García-Ripoll J J, Zoller P and Cirac J I 2003 *Phys. Rev. Lett.* **91** 157901
- [14] Mizrahi J, Neyenhuis B, Johnson K G, Campbell W C, Senko C, Hayes D and Monroe C 2014 *Appl. Phys. B* **114** 45–61
- [15] Hussain M I, Petrasiusnas M J, Bentley C D B, Taylor R L, Carvalho A R R, Hope J J, Streed E W, Lobino M and Kielpinski D 2016 *Opt. Express* **24** 16638
- [16] Madsen M J, Moehring D L, Maunz P, Kohn R N, Duan L M and Monroe C 2006 *Phys. Rev. Lett.* **97** 040505
- [17] Campbell W C, Mizrahi J, Quraishi Q, Senko C, Hayes D, Hucul D, Matsukevich D N, Maunz P and Monroe C 2010 *Phys. Rev. Lett.* **105** 090502
- [18] Mizrahi J, Senko C, Neyenhuis B, Johnson K G, Campbell W C, Conover C W S and Monroe C 2013 *Phys. Rev. Lett.* **110** 203001
- [19] Wong-Campos J D, Moses S A, Johnson K G and Monroe C 2017 *Phys. Rev. Lett.* **119** 230501
- [20] Gerritsma R, Kirchmair G, Zähringer F, Benhelm J, Blatt R and Roos C F 2008 *Eur. Phys. J. D* **50** 13–19
- [21] Ramm M, Pruttivarasin T, Kokish M, Talukdar I and Häffner H 2013 *Phys. Rev. Lett.* **111** 023004
- [22] Jin J and Church D A 1993 *Phys. Rev. Lett.* **70** 3213–3216
- [23] Barton P A, Donald C J S, Lucas D M, Stevens D A, Steane A M and Stacey D N 2000 *Phys. Rev. A* **62** 032503
- [24] Kreuter A, Becher C, Lancaster G P T, Mundt A B, Russo C, Häffner H, Roos C, Hänsel W, Schmidt-Kaler F, Blatt R and Safronova M S 2005 *Phys. Rev. A* **71** 032504
- [25] Taylor R L, Bentley C D B, Pedernales J S, Lamata L, Solano E, Carvalho A R R and Hope J J 2017 *Sci. Rep.* **7** 46197
- [26] Bentley C D B, Carvalho A R R and Hope J J 2015 *New J. Phys.* **17** 103025

- [27] James D F V 1998 *Appl. Phys. B Lasers Opt.* **66** 181–190
- [28] Farrell P M and MacGillivray W R 1995 *J. Phys. A. Math. Gen.* **28** 209–221
- [29] Strickland D and Mourou G 1985 *Opt. Commun.* **56** 219–221
- [30] Agrawal G P and Olsson N A 1989 *IEEE J. Quantum Electron.* **25** 2297–2306
- [31] Manning R J, Ellis A D, Poustie A J and Blow K J 1997 *J. Opt. Soc. Am. B* **14** 3204
- [32] Rizou Z V, Zoiros K E and Connelly M J 2016 *J. Eng. Sci. Technol. Rev.* **9** 198–201
- [33] Guggemos M, Heinrich D, Herrera-Sancho O A, Blatt R and Roos C F 2015 *New J. Phys.* **17** 103001
- [34] Zanon-Willette T, de Clercq E and Arimondo E 2011 *Phys. Rev. A* **84** 062502